

AeroScout UAS Dynamic Analysis

Nathaniel Hollman, Jacob Nobles, Nate Jacobs, Kyron Saunders,
Tiger Sievers, Kaylee Patterson

December 2024

Abstract

This report discusses the efforts made by a group of University of Kansas aerospace engineering students to determine the stability of a small Unmanned Aerial System (UAS) known as the AeroScout. Meticulous measurements taken by the AeroScout group were used as inputs into two computer software applications: Advanced Aircraft Analysis (AAA) and Athena Vortex Lattice (AVL). These measurements along with propeller characteristics and necessary assumptions led to the output of six-degree-of-freedom stability and control derivatives intended to be allocated to the AeroScout under cruise conditions. The trim point found was for steady state rectilinear flight with wings level. These stability and control findings indicate that the aircraft is longitudinally, laterally, and directionally stable and capable of being trimmed. These findings are corroborated by both AAA and AVL.

Nomenclature

AAA = Advanced Aircraft Analysis

AVL = Athena Vortex Lattice

α, β = airflow angles (deg.)

ε = downwash (rad)

i_h = deflection angle of the horizontal stabilizer (deg.)

δa = deflection angle of the ailerons (deg.)

δr = deflection angle of the rudder (deg.)

p, q, r = angular rates (rad/s)

U_1 = steady state flight speed (ft/s)

$C_{L_1}, C_{D_1}, C_{m_1}$ = trimmed condition coefficients (\sim)

C_{L_α} = lift due to α derivative (1/rad.)

C_{y_β} = side force due to β derivative (1/rad.)

C_{l_β} = rolling moment due to β derivative (1/rad.)

C_{m_α} = pitching moment due to α derivative (1/rad.)

C_{n_β} = yawing moment due to β derivative (1/rad.)

$C_{l_{\delta_a}}$ = rolling moment due to δ_a derivative (1/rad.)

$C_{m_{i_h}}$ = pitching moment due to i_h derivative (1/rad.)

$C_{n_{\delta_r}}$ = yawing moment due to δ_r derivative (1/rad.)

C_{l_p} = rolling moment damping derivative (1/rad.)

C_{m_q} = pitching moment damping derivative (1/rad.)

C_{n_r} = yawing moment damping derivative (1/rad.)

S = reference area ($in.^2$)

b = wingspan (in)

c = chord (in)

\bar{c} = mean geometric chord (\sim)

AR = aspect ratio (\sim)

Λ = sweep angle (deg.)

i = incidence angle (deg.)

I = moment of inertia (in^4)

CG = Center of Gravity (\sim)

Contents

1	Introduction	1
2	Methods	2
2.1	Aircraft Geometry Measurement and Recreation	2
2.2	Obtaining Stability and Control Derivatives	3
2.2.1	AAA Assumptions	4
2.3	AAA Compared to AVL	4
2.4	Theory	5
3	Results and Discussion	8
3.1	Aircraft Stability and Trim Criteria	8
3.2	AAA Results	9
3.3	Aircraft Trimmed Flight Condition	11
3.4	AVL Results	11
3.5	Sources of Error and Recommendations	14
4	Conclusions	15
5	Contributions	15
6	Acknowledgments	16
7	Appendix A: Additional Stability and Control Derivative Comparison	18
7.1	AAA	18
7.2	AVL	20

List of Figures

1	Physical Model	2
2	3-View of AAA Model of AeroScout	3
3	α and i_h Graphs from AAA	10
4	Longitudinal and Lateral-Directional Stability Coefficients from AAA	11
5	AVL Model	13
6	α and i_h Graphs from AVL	13
7	Longitudinal and Lateral-Directional Stability Coefficients from AVL	14
8	Airflow Angle Derivatives AAA	18
9	Control Derivatives AAA	18
10	Damping Derivatives AAA	19
11	Steady State Derivatives AAA	19
12	L/D from AAA	19
13	α and i_h Graphs from AAA	20
14	Control Derivatives AVL	20
15	Damping Derivatives AVL	21
16	Steady State Derivatives AVL	21
17	L/D from AVL	21

1 Introduction

The field of study involving UAS stability and control is broader and more demanding than it has been in the past. The race for effective and durable autonomous systems is here and many institutions are heavily invested in research on the stability of UASs. There is currently a persistent demand for fully automated vehicles, and it is far easier to autonomize an inherently stable system than an unstable one. One critical environment where UAS will need to operate is over the ocean, where the wind, along with other adverse conditions, produce ever-changing flight conditions that demand a stable aircraft. These situations are also further complicated by the utilization of UAS swarms, where cooperation and coordination between each system is critical to prevent collisions. These systems are expensive and making them stable can help to reduce some of that cost by simplifying the control algorithm. Some fields of interest currently include non-linear dynamic inversion and adaptive back stepping.

This report produces dynamic analyses of the AeroScout UAS, a remote control plane produced and sold by Horizon Hobby. The dynamic analysis of aircraft is important because it ensures the safety, performance, and reliability of the aircraft. Dynamic analysis provides stability and control derivatives, which can show how an aircraft responds to disturbances such as gusts, turbulence, or sudden control inputs. The derivatives will also indicate if an aircraft will return to steady and controlled flight when such disturbances occur. Advanced Aircraft Analysis [1], developed by DARcorp, and Athena Vortex Lattice (AVL) [2], developed by MIT, are used to input the geometry of the AeroScout and derive stability and control derivatives. AVL and AAA employ different methods for dynamic analysis; by using them in conjunction, it is possible to verify one model against the other. The purpose of this project is to determine these stability and control derivatives of the AeroScout to evaluate the aircraft's stability in 6 degrees of freedom and finally ensure the aircraft can be trimmed for steady-state rectilinear flight.

2 Methods

2.1 Aircraft Geometry Measurement and Recreation

To properly simulate the AeroScout aircraft in software, a detailed digital model must be created. This was accomplished through a process of measuring the components of the aircraft (wing, fuselage, horizontal stabilizer, etc.). These measurements were taken relative to the ground plane (Z distance), the center line of the aircraft (Y distance), and the distance from the nose of the aircraft (X distance). A summary of the aircraft geometry is given in Table 1.

Table 1: AeroScout Geometry Measurements

	Fuselage	Tailboom		Wing	Horizontal Stabilizer	Vertical Tail
Length	15.876 in	23.375 in	Reference Area	324.375 in ²	75.78 in ²	36.5625 in ²
MaxArea	21.342 in ²	4.89 in ²	Span	43.25 in	17.07 in	7.5 in
MaxWidth	3.772 in	4.5 in	Quarter Chord Sweep Angle	1.986 deg	4.46 deg	10.88 deg
MaxHeight	5.9648	2.375 in	Aspect Ratio	5.767	3.84	1.538
			Root Chord	8.0 in	5.0625 in	6.125 in
			Taper Ratio	0.875	0.765	0.592
			Root/Tip Airfoil	NACA 2410	NACA -2410	NACA 64(1)-012



(a) AeroScout RC Plane



(b) Measurement of the Landing Gear

Figure 1: Physical Model

The AeroScout is a small remote control plane constructed with an outer surface of styrofoam. The small size of the aircraft allows for measurements to be made using a tape measure and digital

caliper. Angles were calculated using trigonometry based on measured lengths. All measurements were fed into the AAA software. Next, the airfoil for each planform was selected by overlaying NACA airfoils on an image of the planform wing tip until a match was found. A 3-view was generated in AAA and can be seen in Figure 2. Further, to model the fuselage geometry, pictures of the Aeroscout were taken from a far distance to reduce the effects of perspective, and then these pictures and estimated rho values were used to generate a model in Siemens NX [3]. This model was then used to generate a series of points that could be used to create the fuselage model in AAA. Finally, the center of gravity was initially set at the given specification [4] then adjusted to improve trim performance. The mass of the Aeroscout without a battery was found using a balance and the known battery mass [5] was added.

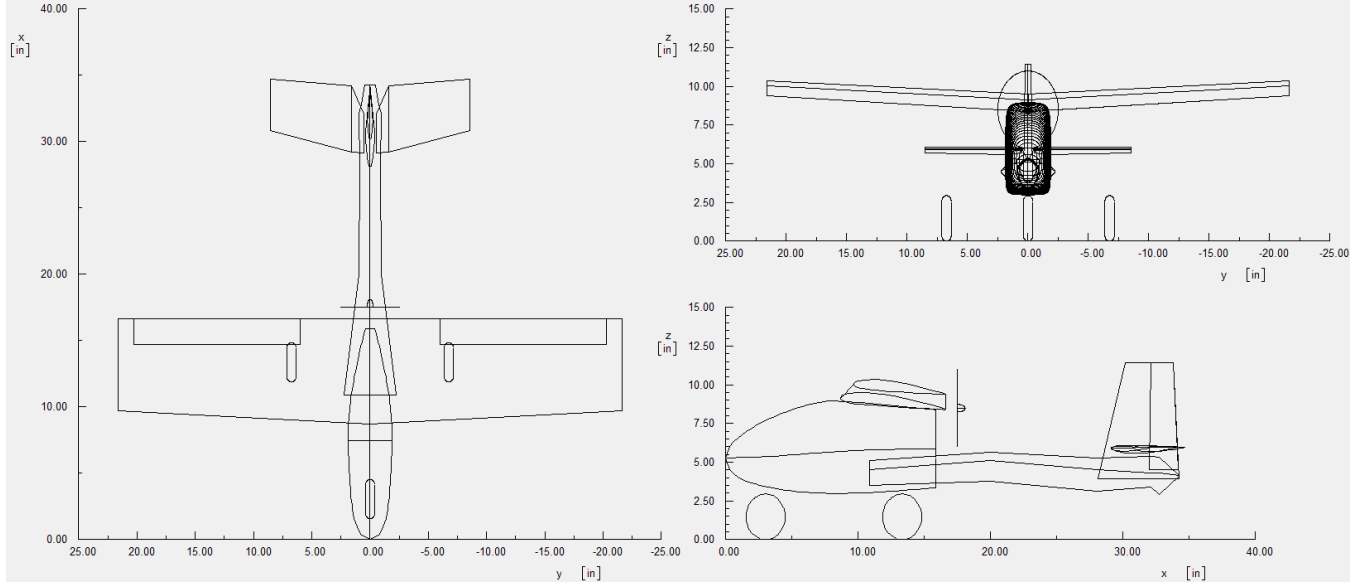


Figure 2: 3-View of AAA Model of AeroScout

2.2 Obtaining Stability and Control Derivatives

Stability and control derivatives are used to relate the effects of translational and rotational movement, airflow angles, and control surface inputs to the total forces and moments acting on the aircraft. The stability derivatives are referred to as such due to their contributions to the stability of an aircraft. When the stability criteria are met, the aircraft will have inherent restoring moments, meaning the aircraft will stop its rotation and return to trim with less need for pilot intervention. Specific examples of these stability conditions are discussed in Section 3.

Control derivatives provide a value to the effects of changing aircraft control surfaces on the aircraft forces and moments. Some of these derivatives can be found by hand using methods such as component build-up, but others can only be calculated in software. Therefore, it was necessary to use the AAA software in determining the dynamic properties of the AeroScout aircraft.

2.2.1 AAA Assumptions

A number of assumptions regarding flight conditions must be made using the AAA software. First, the aircraft is assumed to be in steady-state rectilinear flight at an altitude of 1000 ft above sea-level with a velocity of $35 \frac{ft}{s}$. Additionally, the weights of individual components were not measured and Class I drag was used with the total weight of the aircraft. Since the aircraft is at altitude the ground effects are turned off. Finally, power effects are assumed to be negligible and are therefore turned off.

2.3 AAA Compared to AVL

In combination with the AAA software, AVL was used by four group members to assess and compare the AAA calculated aircraft derivatives. The difference in methodology between the two programs is that AAA uses already collected data for the aerodynamic analysis of each component, or has the needed aerodynamics inputted into the software. Whereas AVL uses the vortex lattice method, using equations to find the discrete aerodynamic forces on each of the defined surfaces. While AAA is usually a more accurate software if all the necessary values are known, AVL is more useful for quick analysis. This is because the only information needed for AVL is the geometry, mass, and flight conditions, and only one function is used to calculate all the necessary variables, simplifying the process and allowing for very fast analysis. AAA takes much longer as each individual variable must be calculated using known variables by groups at a time. This slows down the process but allows for a much more in-depth model with defined individual features. AVL also does not offer as much output data as AAA as the output derivatives, especially drag, are few. AVL also does not allow for the complex modeling of the fuselage, as it can only be approximated using two perpendicular surfaces or a cross-section that builds a circular-section fuselage. It should be noted that these approximated fuselages are then set to only be used for moment derivatives and not forces. Once both sets of data were collected, the averages were compared with values found by each team member.

2.4 Theory

AAA operates based on the theory of component build-up method. By using the geometry input by the group the software can linearize aerodynamic forces and moments. Component build-up takes the individual contributions of planforms and major components of the aircraft to lift, drag, and side force and sums them to find the total coefficients of lift, drag, and sideforce due to the geometry of the aircraft. Component build-up method requires a base. In this case, our base occurs where all control surface deflections and airflow angles are equal to zero. Then essentially, from this base component build-up method is the first order portion of Taylor series expansion.

Lift [6]: In order to find the total coefficient of lift for the aircraft, the component coefficients are added together. C_{L_0} is based on a clean configuration of the aircraft, which is denoted by zero degree α and β , and retracted control surfaces. The coefficient of lift with respect to angle of attack includes the coefficients from the airflow angles of the wing and horizontal tail, where the angle of attack of the horizontal tail is reduced by downwash.

$$C_L = C_{L_{wf}} + C_{L_h} \eta_h \frac{S_h}{S} \quad (1)$$

$$C_L = C_{L_{0wf}} + C_{L_{\alpha wf}} \alpha \quad (2)$$

$$C_{L_h} = C_{L_{0h}} + C_{L_{ah}} \alpha_h \quad (3)$$

$$C_{L_\alpha} = C_{L_{\alpha wf}} + C_{L_{\alpha h}} \eta_h \left(\frac{S_h}{S} \right) \left(1 - \frac{d\varepsilon_h}{d\alpha} \right) \quad (4)$$

$$C_{L_{ih}} = C_{L_{\alpha h}} \eta_h \frac{S_h}{S} \quad (5)$$

$$C_{L_0} = C_{L_{0wf}} - C_{L_{\alpha h}} \eta_h \frac{S_h}{S} \varepsilon_{h0} \quad (6)$$

Drag [1]: The AAA software utilizes our geometry along with estimated values of skin friction coefficients in order to find the total coefficient of drag. First, the program finds skin friction drag and then induced drag due to lift for each component, which makes it possible to then find the total coefficient of drag.

$$C_{D_0} = C_{D_{0wing}} + C_{D_{0v}} + C_{D_{0h}} + C_{D_{trim}} + C_{D_{0fus}} \quad (7)$$

$$C_{D_{0wing}} = R_{wf} R_{I.S.} \left[1 + L'_w \left(\frac{t}{c} \right) + 100 \left(\frac{t}{c} \right)^4 \right] \left[\frac{(C_{fw-lam} - C_{fw-turb}) S_{wet} + C_{tw-turb} S_{wet}}{S} \right] \quad (8)$$

$$C_{D_{0_{fus}}} = (C_{D_{0_f-b}} + C_{D_{b_f}})(1 + K_{install}) \quad (9)$$

$$C_{D_{0_f-b}} = R_{wf} \left[1 + \frac{0.35}{\frac{L_f}{D_{fmax}}} \right] \left[\frac{(C_{flam} - C_{fturb})S_{wet_{flam}} + C_{flam}S_{wet_f}}{S_w} \right] \quad (10)$$

$$C_{D_L} = C_{D_{L_{wing}}} + C_{D_{L_h}} + C_{D_{L_{fus}}} \quad (11)$$

$$C_{D_{L_{wing}}} = \frac{C_{LW}^2}{\pi AR_w e} + 2\pi C_{LW} \varepsilon_{tw} v + 4\pi^2 \varepsilon_{tw}^2 w \quad (12)$$

$$C_{D_{L_{fus}}} = 2a^2 \frac{S_{bf}}{S_w} + \eta c_{dc} |a|^3 \frac{S_{plff}}{S_w} \quad (13)$$

Pitching Moment [1]: Pitching moment is essentially a result of the coefficient of lift with a moment arm involved. The same lifting surfaces are considered along with their distance from the axis of rotation, in the case of pitching moment, this would be the distance from the given surface's aerodynamic center to the x-location of the center of gravity. The theory approximates that the lift is applied at the aerodynamic center of each planform.

$$C_{m_1} = C_{m_0} + C_{m_\alpha} \alpha + C_{m_{i_h}} i_h \quad (14)$$

$$C_{m_0} = C_{m_{0_{wf}}} + C_{m_{0_h}} \quad (15)$$

$$C_{m_{0_{wf}}} = \bar{C}_{m_{0_{wf}}} + C_{L_{0_{wf}}} (\bar{X}_{cg} - \bar{X}_{ac_{wf}}) \quad (16)$$

$$C_{m_{0_h}} = \bar{C}_{m_{0_{wf}}} + C_{L_{0_h}} (\bar{X}_{cg} - \bar{X}_{ac_h}) \quad (17)$$

$$C_{m_\alpha} = -C_{L_{\alpha_{wf}}} (\bar{X}_{cg} - \bar{X}_{ac_{wf}}) - C_{L_{\alpha_h}} (\bar{X}_{ac_h} - \bar{X}_{cg}) \quad (18)$$

When in steady-state rectilinear flight coefficients of lift, drag, and pitching moments are the main concern. If trimming for say, steady-state level turn or pull-up then coefficients of side force, pitching moment, and yawing moment need to be accounted for in a similar fashion using the same theory of component build-up.

Sideforce [6]: When it comes to sideforce, the only part of the plane that component build-up method can be applied to is the vertical tail since it is the only planform contributing majorly to sideforce.

$$C_y = C_{y_0} + C_{y_\beta} \beta + C_{y_{\delta_a}} \delta_a + C_{y_{\delta_r}} \delta_r \quad (19)$$

$$C_{y_\beta} = C_{y_{\beta_w}} + C_{y_{\beta_f}} + C_{y_{\beta_v}} \quad (20)$$

$$C_{y_{\beta_v}} = -C_{L_{\alpha_v}} \left(1 - \frac{d\sigma}{d\beta}\right) \eta_v \left(\frac{S_v}{S}\right) \quad (21)$$

$$C_{y_{\delta_r}} = C_{L_{\alpha_v}} \alpha_{\delta_r} \eta_v \left(\frac{S_v}{S}\right) \quad (22)$$

Rolling Moment [6]: Rolling moments can arise from sideslip or deflection of control surfaces such as the ailerons or rudder. However, none of these factors were present at our analysis trim point. Additionally, the aircraft's symmetrical design ensures that no rolling moment is generated under clean configuration conditions, further supporting the absence of rolling moments in this case.

$$C_l = C_{l_0} + C_{l_\beta} \beta + C_{l_{\delta_a}} \delta_a + C_{l_{\delta_r}} \delta_r \quad (23)$$

The dihedral angle of the wing plays a crucial role in enhancing an aircraft's lateral stability by utilizing geometric design to counteract rolling motions. Dihedral works by increasing the lift produced on the downward-tilted wing during a roll. When the aircraft experiences a sideslip or rolls unintentionally, the lower wing (the wing tilted closer to horizontal due to the roll) encounters a higher effective angle of attack, generating more lift than the opposite wing. This differential lift creates a restoring moment that rolls the aircraft back to its neutral, level position, thereby stabilizing it laterally. In the aircraft being studied, the presence of a dihedral angle contributed to this stabilizing effect. However, under the flight condition analyzed, no rolling moment was observed, due to the absence of any external disturbances or sideslip that would induce a lateral imbalance. This further highlights the importance of dihedral in maintaining stability by automatically correcting for minor lateral disturbances without requiring pilot input. Its role is particularly crucial in smaller, general aviation aircraft, which rely on passive stability features for ease of control.

$$\alpha'_{RW} = \alpha + \Gamma \beta \quad (24)$$

$$\alpha'_{LW} = \alpha - \Gamma \beta \quad (25)$$

$$C_{l_{\beta_h}} = \bar{C}_{l_{\beta_h}} \eta_h \left(\frac{S_h}{S}\right) \left(\frac{b_h}{b}\right) \quad (26)$$

$$C_{l_{\beta_v}} = -C_{l_{\alpha_v}} \beta \left(1 - \frac{\partial \sigma}{\partial \beta}\right) \eta_v \left(\frac{S_v}{S}\right) \left(\frac{z_{vs}}{b}\right) \quad (27)$$

$$C_{l_{\delta_r}} = C_{L_{\alpha v}} \tau_{\delta_r} \eta_v \left(\frac{S_v}{S} \right) \left(\frac{z_{vs}}{b} \right) \quad (28)$$

Yawing Moment [6]: Yawing moment can also be generated from sideslip, aileron deflection angles, and rudder deflection angles. When incurring sideslip, the relative airflow over the wings creates a pressure differential on the vertical tail and fuselage, inducing a moment. During aileron deflection, a similar phenomena occurs where the differing angles of deflection cause a pressure difference and induce a yawing moment. In the case analyzed, the symmetrical design results in no yawing moment under clean configuration.

$$C_n = C_{n_0} + C_{n_\beta} \beta + C_{n_{\delta_a}} \delta_a + C_{n_{\delta_r}} \delta_r \quad (29)$$

$$C_{y_\beta} = C_{n_{\beta_w}} + C_{n_{\beta_f}} + C_{n_{\beta_v}} \quad (30)$$

$$C_{n_{\beta_v}} = C_{n_{\alpha v}} \beta \left(1 - \frac{\partial \sigma}{\partial \beta} \right) \eta_v \left(\frac{S_v}{S} \right) \left(\frac{x_{vs}}{b} \right) \quad (31)$$

$$C_{n_{\delta_r}} = -C_{L_{\alpha v}} \tau_{\delta_r} \eta_v \left(\frac{S_v}{S} \right) \left(\frac{x_{vs}}{b} \right) \quad (32)$$

3 Results and Discussion

3.1 Aircraft Stability and Trim Criteria

From the AAA data, average values of stability and control derivatives were derived. These stability derivatives describe how an aircraft will behave when in flight. The sign of the stability derivatives will determine if the AeroScout is stable in rectilinear flight, corresponding to the convention of the textbook [6]. For example, C_{n_β} must be positive, as this will cause the aircraft to yaw into incoming flow and reduce side slip. A negative value of C_{n_β} would cause the aircraft to yaw away from the incoming flow, increasing side slip and causing instability. C_{m_α} must be negative for longitudinal stability. In flight, an aircraft may encounter gusts of wind that cause the aircraft to pitch up and increase alpha, which increases lift. A negative C_{m_α} will cause a restoring moment and cause the aircraft to pitch back down, returning to stable flight. For lateral stability, C_{l_β} must be negative. When an aircraft experiences sideslip, the wings and fuselage experience asymmetrical airflow. A negative C_{l_β} will cause the aircraft to roll away from the sideslip and back to level flight. C_{l_p} describes how the rolling moment changes in response to a roll rate, p . For lateral stability, C_{l_p}

must be negative to contribute to roll damping and prevent any further rolling. A negative C_{m_q} is required for longitudinal stability, as this will cause a restoring moment in the case of the aircraft pitching up or down. C_{n_r} must be negative to cause a restoring yawing moment when the aircraft yaws in either direction. Table 2 shows stability derivatives found by each team member and the average values.

When trimming the AeroScout, two important values acquired are the required angle of attack, α , and incidence angle of the elevator, i_h . The angle of attack required is that needed to generate enough lift that the lift is equal to the weight of the aircraft. When the trim alpha is met, the lift of the wings creates a moment about the center of gravity. To counteract this moment, the incidence angle of the horizontal stabilizer is trimmed such that it creates an equal and opposite moment. The combined effect of these allows the aircraft to fly in steady, rectilinear flight. So, for trim condition:

$$M_{A/C} = M_{wing} + M_{incidence\ angle} = 0 \quad (33)$$

3.2 AAA Results

Average and individual values from the AAA models are provided in Table 2. The angle of attack and horizontal stabilizer incidence graph is shown in Figure 3. The stability and control derivatives are shown in Figure 4.

The results of the AAA analysis on the AeroScout showed that the aircraft has reasonable dynamic flight characteristics and is stable. Steady-state coefficients were also found to be reasonable since they lead to a relatively high lift-to-drag ratio for a radio-control aircraft. An average was taken for each team member's analysis for each derivative and trim value. The average showed $C_{m_\alpha} = -1.5473 \text{ rad}^{-1}$, $C_{l_\beta} = -0.4983 \text{ rad}^{-1}$, and $C_{n_\beta} = 0.0331 \text{ rad}^{-1}$. The sign conventions of these derivatives indicate the aircraft was longitudinally, laterally, and directionally stable as explained in section 3.1.

The aircraft was also stable in perturbed steady-state flight, as the average rotational derivatives were $C_{l_p} = -0.4263 \text{ rad}^{-1}$, $C_{m_q} = -12.269 \text{ rad}^{-1}$, and $C_{n_r} = -0.0583 \text{ rad}^{-1}$, which follows the previously mentioned rules for stability. These derivatives are supposed to be negative because if there is a positive rate of perturbed pitch, roll, or yaw then a negative coefficient would restore that positive rate and bring the aircraft back to equilibrium. It was found that $C_{L_\alpha} = 4.9873 \text{ rad}^{-1}$,

Table 2: Trimmed flight conditions and stability and control derivatives from AAA.

	Average	Jacob	Kaylee	Kyron	Nate	Nathaniel	Tiger
V (ft/s)	37.5	35	40	40	35	40	35
α (deg)	-1.0945	-0.4600	-2.3700	-1.7800	0.4600	-1.8670	-0.5500
i_h (deg)	-0.3300	-0.5000	3.7000	1.1000	-5.4000	-1.1800	-1.6000
SM (%)	26.6450	16.51	3.91	24.89	34.93	52.64	26.99
$C_{L\alpha}$	4.9874	4.9873	4.9870	4.9875	4.9877	4.9870	4.9878
$C_{y\beta}$	-0.2233	-0.2667	-0.2177	-0.2157	-0.1818	-0.2226	-0.2350
$C_{I\beta}$	-0.4983	-0.4952	-0.5016	-0.4904	-0.5001	-0.4810	-0.5213
$C_{m\alpha}$	-1.5473	-0.2460	-0.1951	-4.7481	-1.7416	-1.1100	-1.2431
$C_{n\beta}$	0.0331	0.0468	0.0263	0.0318	0.0194	0.0340	0.0401
$C_{l\delta a}$	0.3302	0.3296	0.3296	0.3330	0.3296	0.3296	0.3296
C_{mih}	-2.2474	-2.1205	-2.1130	-2.2962	-2.3851	-2.2730	-2.2968
$C_{n\delta r}$	-0.0345	-0.0494	-0.0362	-0.0389	0.0022	-0.0407	-0.0442
$C_{I\rho}$	-0.4263	-0.4258	-0.4257	-0.4254	-0.4280	-0.4237	-0.4291
C_{mq}	-12.2687	-10.8421	-10.7828	-12.6063	-13.7588	-13.0070	-12.6149
C_{nr}	-0.0583	-0.0668	-0.0493	-0.0565	-0.0501	-0.0536	-0.0733
C_{L1}	0.4785	0.5036	0.4316	0.4131	0.4851	0.3700	0.6673
C_{D1}	0.0952	0.1468	0.0717	0.0538	0.1002	0.0564	0.1420
C_{m1}	0.0584	0.1426	-0.0184	0.0000	0.0820	0.1229	0.0215
L/D	5.0284	3.4305	6.0195	7.6784	4.7149	6.5603	4.6993

with a high consistency between data points, with a maximum deviation of 0.0008.

Variations in results between team members are due to a multitude of differences between input values. These include but are not limited to center of gravity x-locations ranging from 9 in. from the nose to nearly 13 in, velocity ranges from 35 ft/s to 40 ft/s, a range of altitudes, and other smaller compounding assumptions. While the results across the team were similar overall changing design parameters and flight conditions cause noteworthy differences in numerical values.

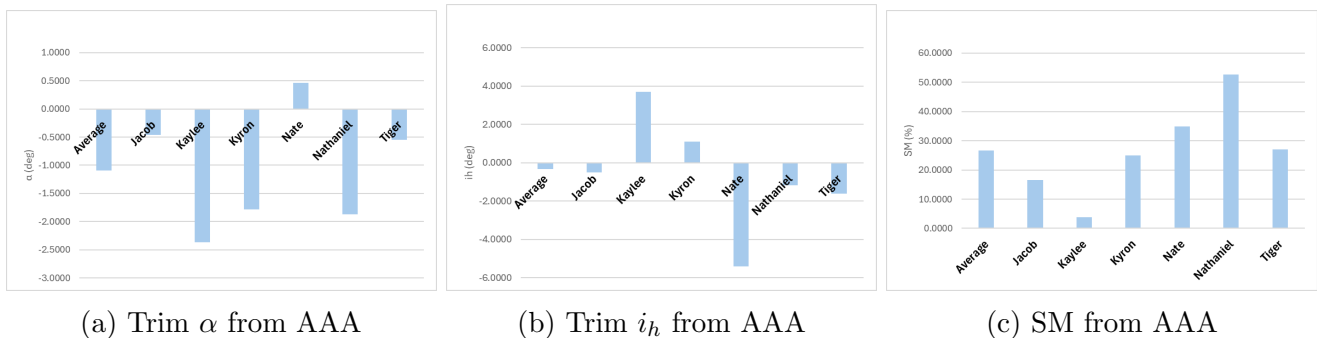
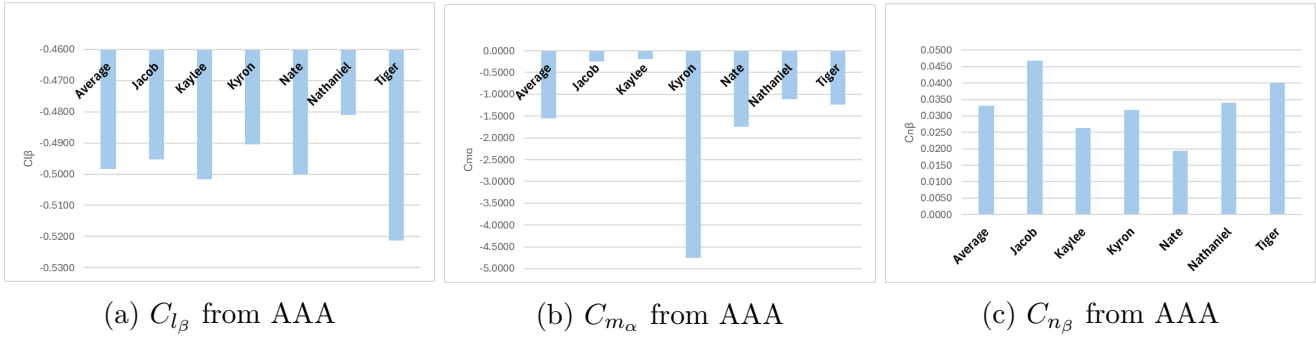


Figure 3: α and i_h Graphs from AAA



(a) $C_{l\beta}$ from AAA (b) $C_{m\alpha}$ from AAA (c) $C_{n\beta}$ from AAA

Figure 4: Longitudinal and Lateral-Directional Stability Coefficients from AAA

3.3 Aircraft Trimmed Flight Condition

From Table 2, the average required angle of attack to trim is $\alpha = -1.0945^\circ$. A negative α indicates that the AeroScout generates excess lift at $\alpha = 0^\circ$. This is supported by the fact that the AeroScout wings have a positive incidence angle, as seen in Figure 2. The average required incidence angle of the horizontal stabilizer is $i_h = -0.33^\circ$. This incidence angle indicates that in trimmed, rectilinear flight, the AeroScout wants to pitch nose down. A negative incidence angle in the horizontal stabilizer causes a positive pitching moment and returns the aircraft to rectilinear flight. Moving the center of gravity of the aircraft aft will reduce the required incidence angle. Additionally, if a positive incidence angle can be achieved, the overall angle of attack will decrease due to positive incidence angle creating a favorable trim condition.

These values of α and i_h are within desired ranges. A negative α_{trim} means that, if needed, a higher angle of attack can be acquired and generate more lift. If α_{trim} were positive, there would be less available deflection before the aircraft reaches stall. The required i_h for trim condition is relatively small and leaves excess incidence angle available in either direction. Excess available incidence angle proves useful when the aircraft experiences outside longitudinal forces, such as turbulence or sudden gusts of wind.

3.4 AVL Results

The AVL model can be seen in Figure 5. Average and individual values from the AVL models are provided in Table 3 in addition to a comparison to the average AAA values. The angle of attack and horizontal stabilizer incidence graph is shown in Figure 6. The stability and control derivatives are shown in Figure 7.

Table 3: Trimmed flight conditions and stability and control derivatives from AVL.

	Variance from AAA	AAA Average	AVL Average	Jacob	Kyron	Nathaniel	Tiger
V (ft/s)	~	37.5	37.5	35	40	40	35
α (deg)	-172.66%	-1.0945	0.7953	1.8441	-0.9831	-0.2535	-1.1100
i_h (deg)	-190.26%	-0.3300	-0.9579	-1.5457	-0.0036	-0.3700	-3.1100
SM (%)	33.40%	26.6450	35.55	41.33	36.13	29.82	34.90
$C_{L\alpha}$	4.69%	4.9874	4.7537	4.6714	4.6643	4.8360	4.7592
$C_{y\beta}$	-63.67%	-0.2233	-0.3654	-0.2730	-0.2679	-0.4578	-0.2687
$C_{I\beta}$	-79.80%	-0.4983	-0.1007	-0.0988	-0.0917	-0.1025	0.0000
$C_{m\alpha}$	-8.98%	-1.5473	-1.6863	-1.9305	-1.6852	-1.4420	-1.6611
$C_{n\beta}$	153.67%	0.0331	0.0839	0.0793	0.0559	0.0885	0.0555
$C_{l\delta_a}$	103.15%	0.3302	-0.0104	-0.0103	-0.0104	-0.0105	0.0000
C_{mih}	-99.97%	-2.2474	-0.0007	-0.0012	-0.0002	-0.0002	-0.0002
$C_{n\delta_r}$	-105.56%	-0.0345	0.0019	0.0019	0.0020	0.0019	0.0000
C_{lp}	-7.10%	-0.4263	-0.4566	-0.4517	-0.4591	-0.4614	-0.4716
C_{mq}	-3.32%	-12.2687	-11.8608	-12.6475	-12.0295	-11.0740	-12.0910
C_{nr}	-154.17%	-0.0583	-0.1481	-0.1525	-0.1380	-0.1437	-0.1376
C_{L1}	12.87%	0.4785	0.5400	0.6248	0.4381	0.4553	0.4381
C_{D1}	45.82%	0.0952	0.0516	0.0275	0.0129	0.0757	0.0140
C_{m1}	100.00%	0.0584	0.0000	0.0000	0.0000	0.0000	0.0000
L/D	108.34%	5.0284	10.4759	22.7603	34.0148	6.0185	31.3383

Along with the AAA models created, four AVL models were developed to expand the dataset and provide a second source of analysis for comparison. Since AVL and AAA use different approaches to aerodynamic and stability analysis, comparing their outputs helps identify the limitations and strengths of each model. This cross-verification will help in determining whether the methodologies employed by each software is reliable. From the comparison tables above, several discrepancies were observed between the outputs of the AAA and AVL models. The data set was average, and percent error were calculated to identify the most significant differences. While some stability outputs showed large differences, it is essential to note that these are average comparisons; the actual values often remain within the ranges of each other. This overlap suggests that despite their methodological differences, both models capture key insights with reasonable accuracy. Through this analysis, it is evident that having multiple sources of data provides insights into the model's accuracy.

The largest percent differences between the average values were found with $C_{n\beta}$ and C_{nr} with differences of 153.67% and -154.17% respectively. This could be due to how the model's geometry was created, with the AVL fuselage's being created using two flat planes to approximate the size and shape, while AAA used more detailed fuselage modeling. This could also be caused by other

assumptions made by both models when assuming values like skin friction and induced vortices.

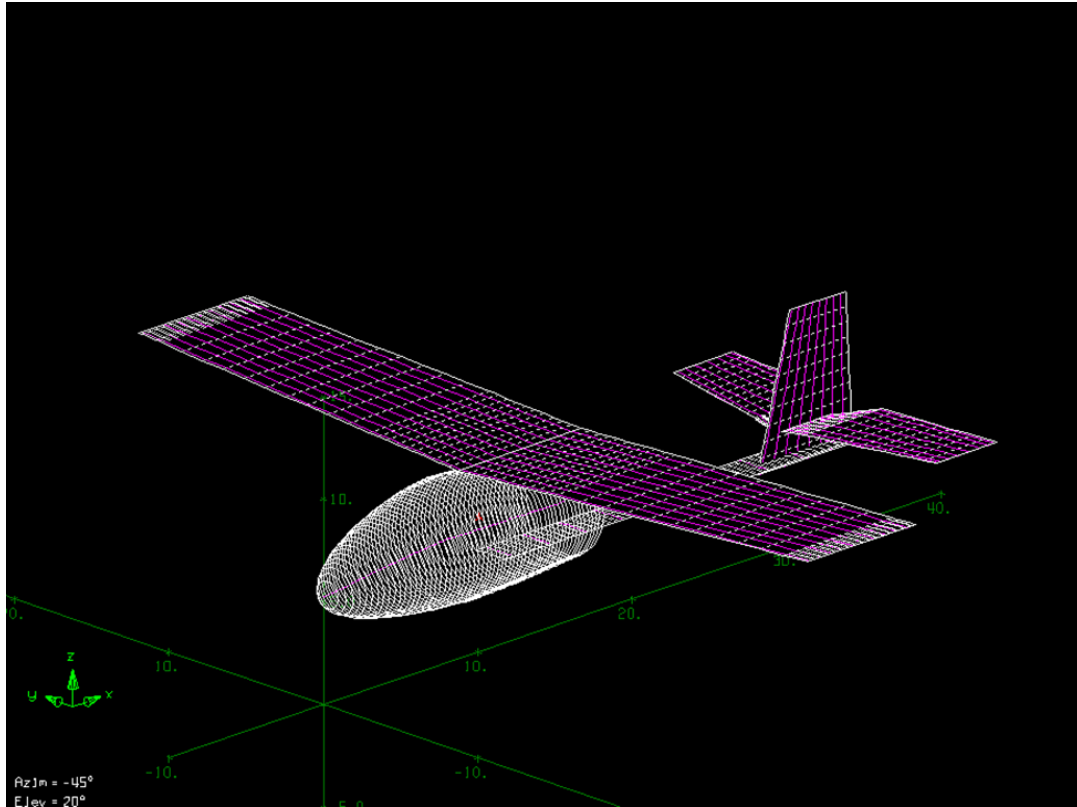


Figure 5: AVL Model

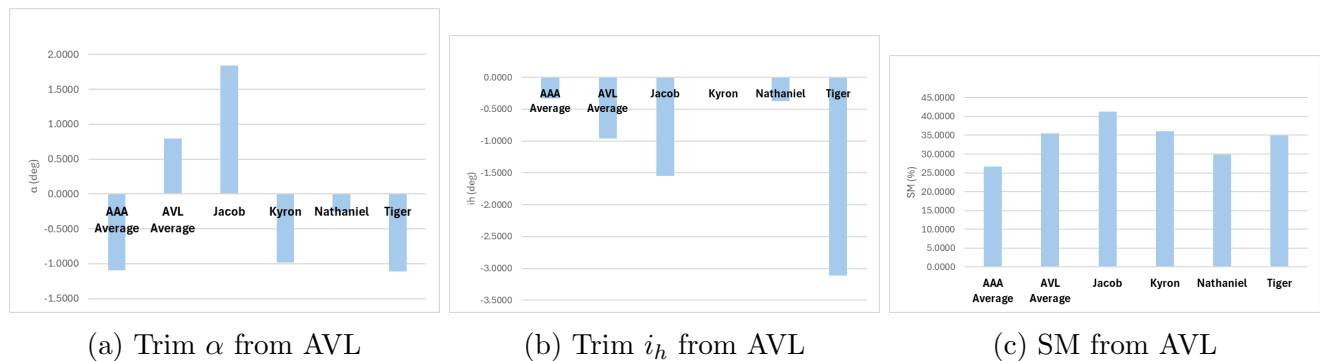


Figure 6: α and i_h Graphs from AVL

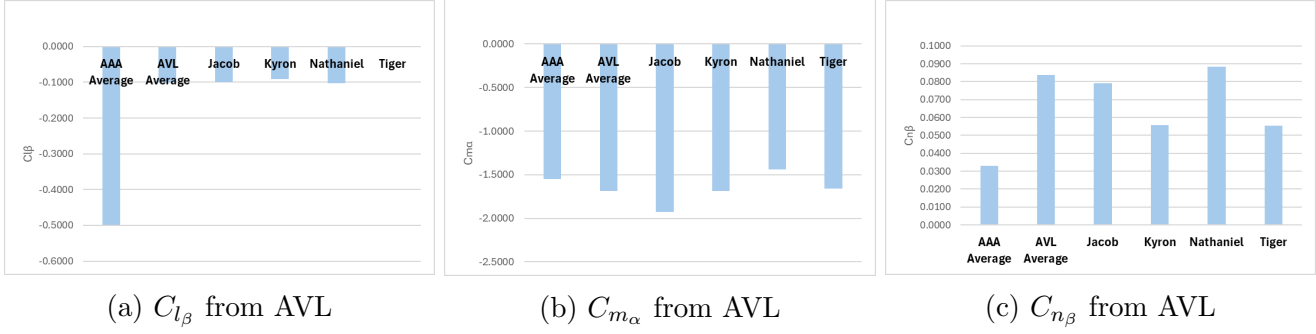


Figure 7: Longitudinal and Lateral-Directional Stability Coefficients from AVL

3.5 Sources of Error and Recommendations

There are several sources of error in data acquisition and AAA methods that may contribute to variance between individual team member's AAA models. The main contributions are measurement precision with the available tools. One example of this is the inaccuracy in fuselage plus tailboom length due to the measurement datum plan. Another example is lifting surface incidence and dihedral angles which, using length measurements that had inherent error, will also have error angles acquired from trigonometry. With the AAA models, there was variation with how aerodynamics was calculated for each team member's AAA model, specifically variables related to lift and drag due to individual components in the model. Stability and control derivatives directly related to aerodynamics will deviate due to this variation. A final source of error might come from how mass and moment of inertia were calculated and the placement of center of gravity. The actual values may differ from the AAA models due to the relatively simple method of acquiring these values. With the AVL model, Nathaniel was the only team member to more accurately model the fuselage of the aircraft while the rest of the team utilized flat sheets to approximate the fuselage geometry.

These deviations and inaccuracies can be mitigated by taking average values and validating values across different software models. The work outlined in this report underscores the importance of using diverse stability and control analysis methods to enhance reliability in aerodynamic predictions. It is recommended that future research focus on standardizing inputs, integrating experimental data, conducting sensitivity analyses, and automating analysis processes to further improve accuracy and efficiency in design. With more coordination in model creation and targeted modifications to each model showing outlier values, the models could be better validated.

4 Conclusions

The AeroScout was found to be stable through two different computer aided stability analyses and several resultant criterion discussed in section 3. While AAA and AVL did not produce identical results the conclusions from the analyses are the same: the aircraft is stable and can be trimmed. The AAA and AVL analysis provided valuable insight into the aerodynamic and stability characteristics of the model. Overall, despite a variety of velocities and other input variables, the group members' models each found the aircraft to be stable.

The consistency of these results will allow these models to be used as a low-fidelity base for developing a more optimal system. From this base, iterative development and more advanced simulation efforts can be undertaken. These findings and the methods presented herein can be used to further optimize this aircraft, and similar techniques can be applied to aid the development of other stable UASs.

5 Contributions

While all members contributed to review and formatting, specific individual efforts of the group members are recorded below.

Name	Contributions
Jacob	AAA + AVL Analysis, Geometry, Summary Tables, AAA Assumptions
Kaylee	AAA Analysis, Intro, Conclusion, Abstract, Results Discussion, Theory
Kyron	AAA + AVL Analysis, Plots, Sources of Error, Measurements, Theory
Nate	AAA Analysis, Stability and Trim Criteria, Trimmed Flight Condition
Nathaniel	AAA + AVL Analysis, Excel Generation, References, AAA Results, AAA vs AVL
Tiger	AAA + AVL Analysis, AVL Results, Nomenclature, Conclusion, Theory

Table 4: Team Member Contributions

6 Acknowledgments

The authors of this report would like to show their gratitude for the advice, encouragement, and help of the professor, Dr. Shawn Keshmiri, and the graduate teaching assistant, Muhammad Hakawu. Special thanks are also given to the doctoral candidates, Justin Clough and Megan Carlson, for dedicating some of their valuable time to teaching the class the AAA and AVL software and giving guidance on how to use them.

References

- [1] “Advanced Aircraft Analysis” Version 5.1. Design, Analysis, and Research Corporation, Lawrence, KS, 2023.
- [2] “Athena Vortex Lattice” Version 3.4, Massachusetts Institute Technology, Cambridge, MA, 2023.
- [3] “NX” Version 2406, Siemens, Munich, Germany, 2024.
- [4] Horizon Hobby. ”AeroScout S 2 1.1m Instruction Manual.” *Horizonhobby.com*, 2022.
- [5] Horizon Hobby. ”1.11V 2200mAh 3S 30C Smart LiPo Battery: IC3,” *Horizonhobby.com*, 2024.
- [6] Roskam, J., “Airplane Flight Dynamics and Automatic Flight Controls” 7th Edition, Design, Analysis and Research corporation, Lawrence, Kansas, 2018.

7 Appendix A: Additional Stability and Control Derivative Comparison

7.1 AAA

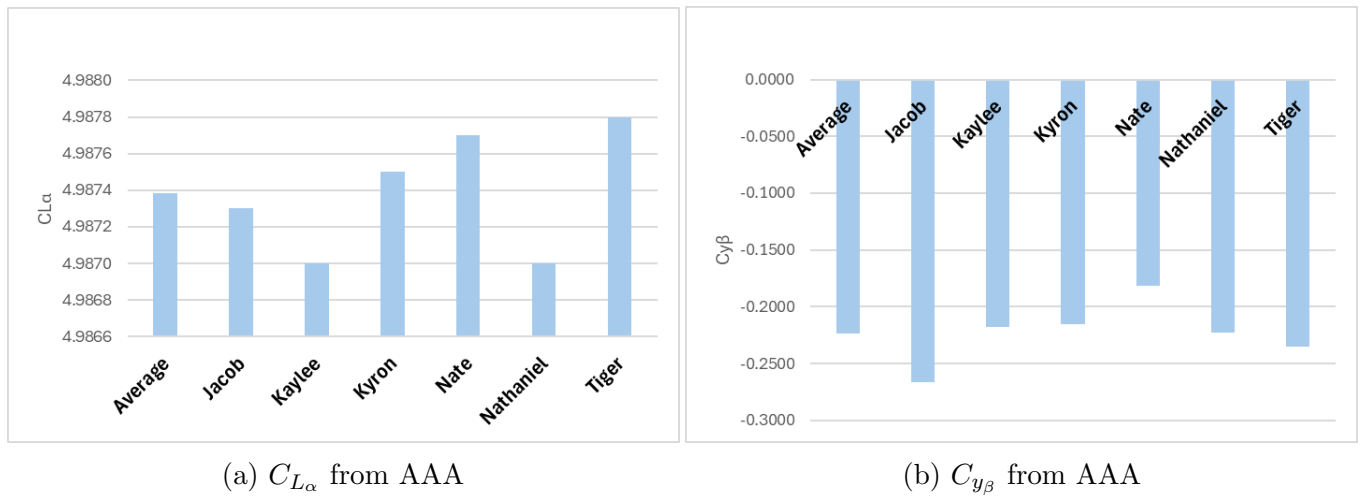


Figure 8: Airflow Angle Derivatives AAA

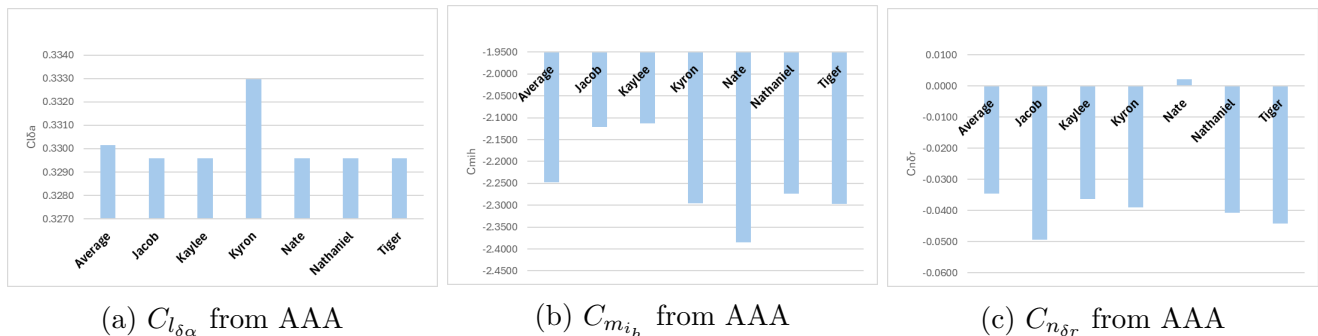
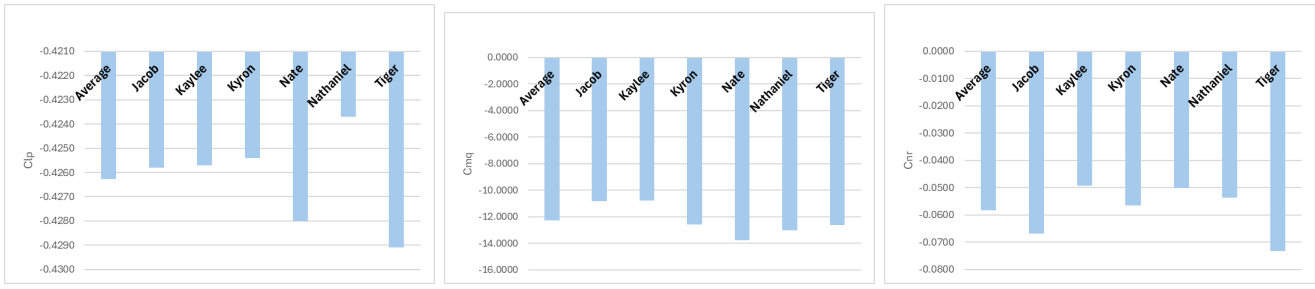


Figure 9: Control Derivatives AAA

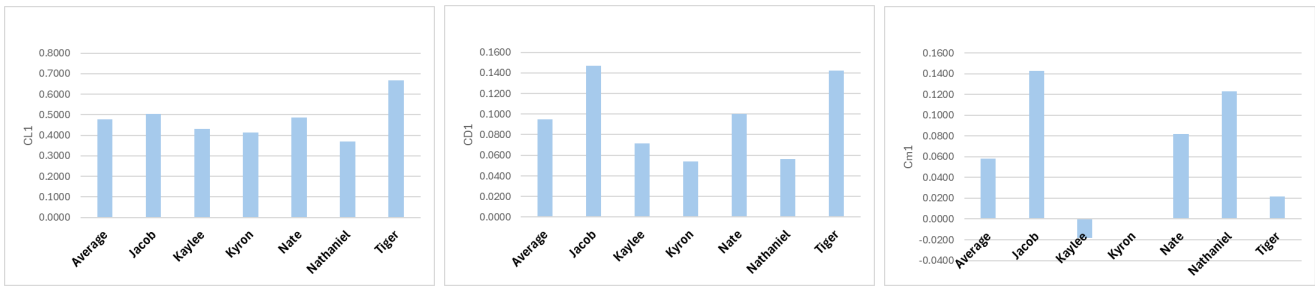


(a) C_{l_p} from AAA

(b) C_{m_q} from AAA

(c) C_{n_r} from AAA

Figure 10: Damping Derivatives AAA



(a) C_{L_1} from AAA

(b) C_{D_1} from AAA

(c) C_{m_1} from AAA

Figure 11: Steady State Derivatives AAA

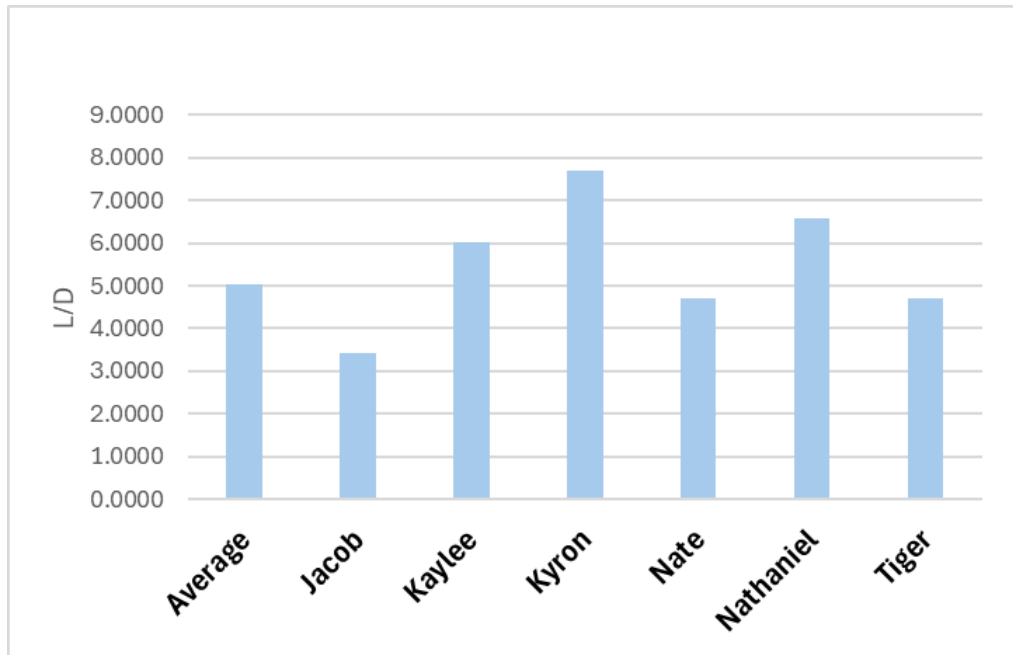


Figure 12: L/D from AAA

7.2 AVL

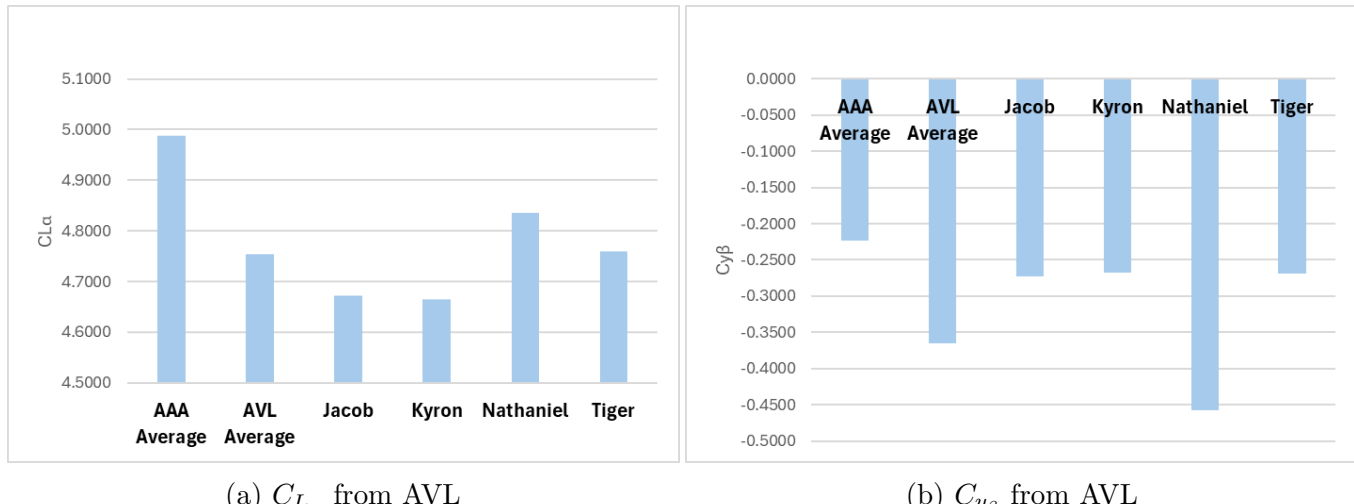


Figure 13: α and i_h Graphs from AAA

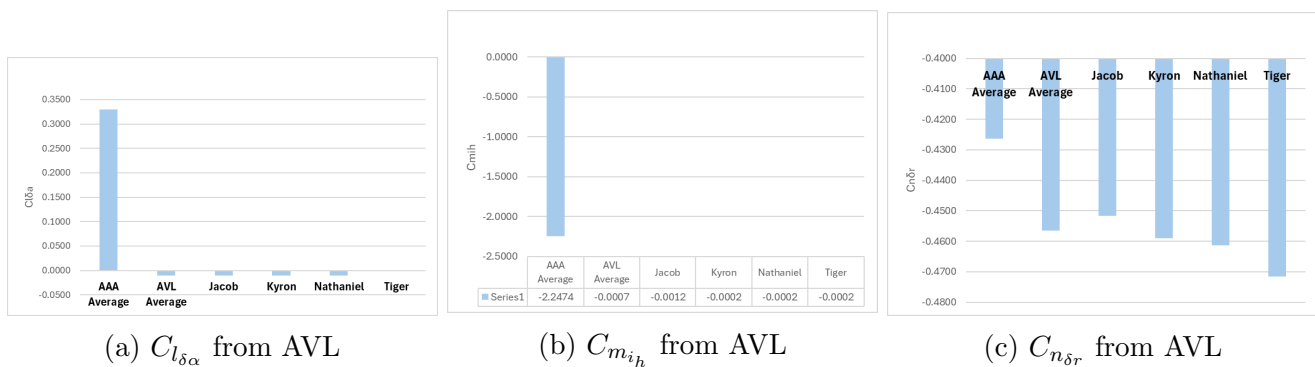


Figure 14: Control Derivatives AVL

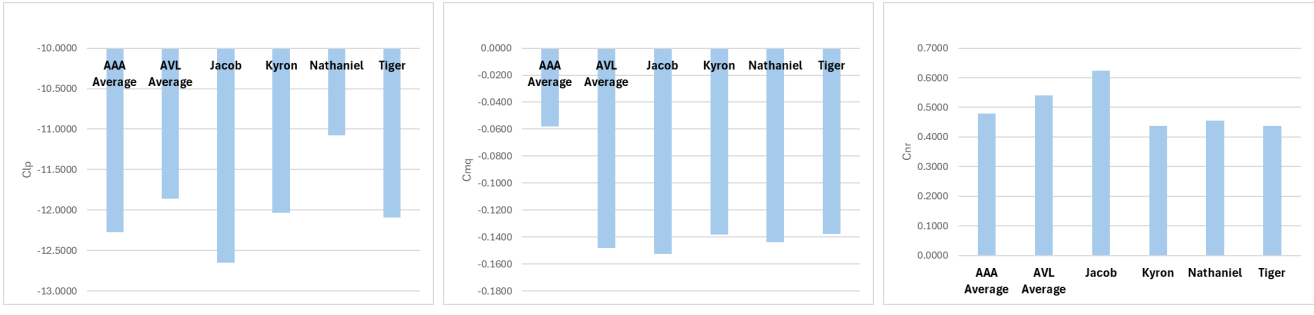
(a) C_{l_p} from AVL(b) C_{m_q} from AVL(c) C_{n_r} from AVL

Figure 15: Damping Derivatives AVL

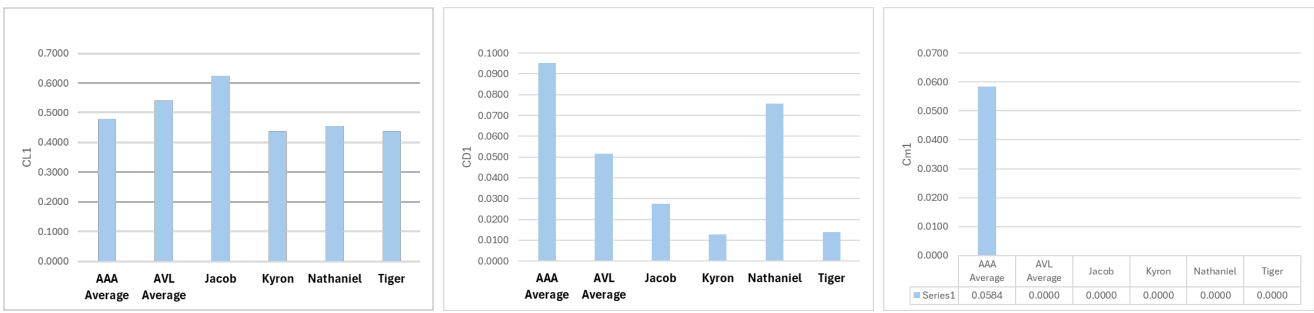
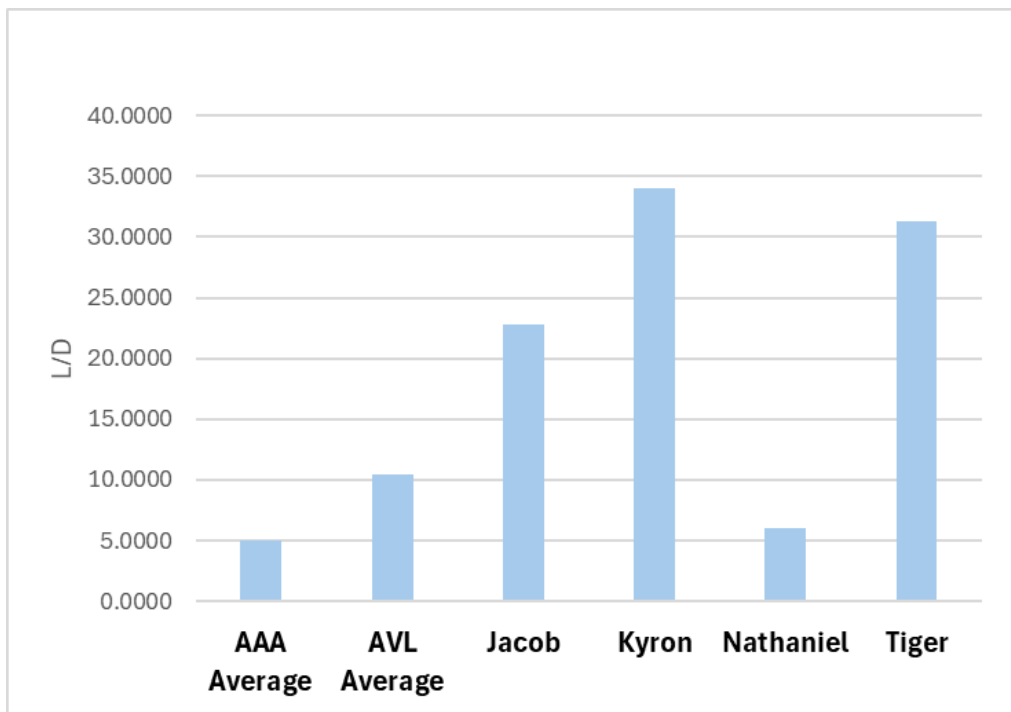
(a) C_{L_1} from AVL(b) C_{D_1} from AVL(c) C_{m_1} from AVL

Figure 16: Steady State Derivatives AVL

Figure 17: L/D from AVL